Adaptive Super-Twisting Controller for Voltage Regulation in a DC Microgrid

Mehdi Ashtari Mahini[1,*], Seyed Mehdi Hakimi[2], Seyed Vahid Naghavi[3], and Vahid Behnamgol[4]

[1] *Department of Electrical Engineering, Damavand Branch, Islamic Azad University, Tehran, Iran*
[2] *Department of Electrical Engineering and Renewable Energy Research Centre. Damavand Branch, Islamic Azad University, Tehran, Iran.*
[3] *Research Institute of Petroleum Industry.*
[4] *Malek Ashtar University of Technology.*
**Corresponding author: mahdi.ashtari60@gmail.com*

Manuscript received 24 October, 2025; revised 12 June, 2026; accepted 20 June, 2026. Paper no. JEMT-2510-1577

Microgrids (MGs) typically function in two operational modes: on-grid and off-grid. The primary challenges in the off-grid mode involve voltage and frequency fluctuations or instability. To address these issues, an appropriate control system is required to regulate the microgrid's voltage and frequency. Considering the system's nonlinear characteristics, parameter uncertainties, and load variations, the use of nonlinear and robust control techniques is deemed an effective strategy. In this study, a nonlinear adaptive super-twisting controller based on sliding mode control (SMC) theory is developed to manage the microgrid. The main motivation for employing this controller is its ability to mitigate distortions under parameter uncertainties. To this end, the dynamic equations of the system are first derived, and subsequently, a controller is designed using the principles of SMC to ensure overall system control. To overcome the chattering phenomenon, an adaptive super-twisting algorithm is proposed. The closed-loop stability of the system is verified through the Lyapunov stability theorem. The effectiveness of the proposed method is assessed using MATLAB/Simulink simulations, and its performance is compared with conventional control approaches. The results demonstrate that the proposed adaptive super-twisting controller offers superior performance and practical applicability compared to traditional methods. The proposed controller is evaluated in an islanded (off-grid) DC microgrid configuration under load steps, irradiance variations, and battery parameter uncertainties. Simulation results demonstrate superior voltage regulation compared to a conventional super-twisting sliding mode controller and a PI controller, achieving a settling time below 0.18 s, an overshoot below 0.4%, and an RMSE of 0.42 V.

Keywords: *microgrid, voltage regulation, nonlinear control, second order sliding mode control, super-twisting method*

http://dx.doi.org/10.22109/jemt.2026.555273.1577

Nomenclature

sets

t	Time
i	MGs number
Parameters and variables	
C_i	Capacitance of capacitor i in the DC microgrid (f)
$d, d_1 - d_4$	Model and parametric uncertainties for each subsystem
$\hat{d}$	Estimated value of uncertainty
e	Tracking error between reference and measured signal
$f(x)$	Known part of nonlinear dynamic function vector
$g(x)$	Uncertain nonlinear function vector
$I_L, I_{L3}, I_{L6}, I_{L9}, I_{L13}$	Inductor or load current in converter subsystem (A)
I_L^*, I_{L9}^*	Reference current signal (A)
I_{PV}	PV array current (A)
k_1, k_2	Super-twisting controller gains
L_i	Inductance in converter subsystem (H)
$P_{bat}, P_{load}, P_{PV}, P_{SC}$	Battery, load, PV, and super-capacitor power (W)
R	Equivalent resistance of element or load
s	Sliding surface (sliding function)
$\dot{s}$	Time derivative of sliding variable

T_r	Reaching time of sliding motion
$u, u_1 - u_4$	Control input of the system or each converter
V_{dc}	DC-link voltage (V)
V_{ref}	Reference DC voltage (V)
$V_{C1}, V_{C2}, V_{C4}, V_{C5}, V_{C7}, V_{C8}, V_{C11}, V_{C12}$	Capacitor voltages in converters (V)
V_{C2}^*, V_{C11}^*	Desired (reference) capacitor voltages (V)
V_{PV}	PV output voltage (V)
x	State vector of system
$\dot{x}$	Time derivative of state vector
V	Lyapunov function candidate
$\dot{V}$	Time derivative of Lyapunov function
α	Adaptation gains in adaptive super-twisting algorithm
β	Auxiliary adaptive or design parameter
λ_1, λ_2	Positive adaptation rates for uncertainty estimation
ρ	Upper bound of system uncertainty
$\dot{\rho}$	Upper bound of derivative of uncertainty
σ	Sliding variable
$\dot{\sigma}$	Time derivative of sliding variable
η	Positive design constant used in Lyapunov inequality
μ	Controller tuning coefficient (if appearing in adaptive law)
κ	Gain coefficient ensuring finite-time stability

1. Introduction

A MG is a small-scale power network designed to supply electricity to residential communities and small industrial facilities. It can operate either in on-grid or off-grid mode. An MG typically comprises distributed generators (DGs), loads, and energy storage devices such as batteries and supercapacitors. The growing demand for microgrids stems from their numerous economic and geographical advantages, which have driven the development of more practical and flexible configurations. Energy generation sources within microgrids include wind turbines, fuel cells, photovoltaic (PV) systems, and batteries, while the connected loads may require either AC or DC power. In on-grid mode, the main grid is responsible for maintaining voltage and frequency stability, and the MG primarily serves as a supplementary power source. Conversely, in off-grid mode, the MG must regulate its voltage and frequency autonomously using appropriate control strategies, as it operates independently of the main grid. Given their increasing deployment, both on-grid and off-grid microgrids play a vital role in enhancing system stability and operational efficiency. As such, an MG can be viewed as a controllable dynamic system, where voltage, current, and frequency outputs are regulated by suitably designed input control signals. Various control methodologies have been proposed for MGs, each with distinct advantages and limitations. Linear controllers—due to their structural simplicity and ease of implementation—have been widely adopted in early MG applications. However, their performance deteriorates in the presence of system nonlinearities and parametric uncertainties [1], [2]. Moreover, the growing deployment of DC microgrids is closely linked to broader environmental and economic imperatives. Improved power conversion efficiency in DC microgrids directly reduces curtailment of renewable generation, thereby lowering lifecycle carbon emissions [3], [4]. The integration of battery storage and floating PV systems introduces additional environmental considerations related to lifecycle assessment [5], [6]. At the system level, robust voltage regulation reduces energy waste and supports the economic viability of islanded communities that rely on off-grid power [7], [8]. These motivations underscore the importance of developing advanced control strategies that combine high performance with practical implement ability.

To overcome these limitations, more advanced approaches such as modern control and state feedback control have been explored for AC microgrids. Unlike conventional PID controllers, state feedback methods utilize the internal dynamics of the system, resulting in enhanced performance [9]. Nonetheless, these methods often require complete state measurements and fail to account for uncertainties and nonlinear behaviors. Similar linearized feedback control strategies have been applied to converter regulation in MGs in [10] and [11].

In recent years, efforts to improve MG control performance have focused on hybrid approaches, integrating classical PID control with modern control theories. For instance, a PID–LMI-based robust controller has been employed for voltage regulation in MGs [12], while an adaptive PID controller has been designed for voltage and current control [13]. Additionally, fuzzy-PID methods have been implemented for power regulation in MGs with storage batteries [14], and fractional-order PID controllers have been proposed for frequency control [15]. Further developments include combining linear state feedback with robust control techniques for on-grid applications [16], and integrating LQR and robust control for simultaneous voltage and frequency regulation in PV–battery-based MGs [17]. Moreover, classical robust control frameworks have also been utilized for microgrid control and stabilization [18].

In robust control strategies, nonlinear systems are typically transformed into an equivalent linear model supplemented by an uncertainty boundary term. The controller is then designed to handle the worst-case scenario within this uncertainty range. Although effective in ensuring system robustness, this approach often results in large control efforts, which may exceed the actuator's operational limits. To enhance performance and adaptability, robust control has been integrated with adaptive control techniques for MG applications [19]. In addition to model-based approaches, several intelligent control methods—which do not require an explicit system model—have been proposed for MG regulation. Notably, hybrid fuzzy-neural controllers have been applied for microgrid control in [20]– [22]. Similarly, a fuzzy intelligent approach combined with comparative control theory was presented in [23], and a fractional-order fuzzy hybrid controller was developed for real-time frequency regulation in [24]. In recent years, nonlinear control methods have gained significant attention for MG control due to their ability to address system nonlinearities and uncertainties directly. Several studies have employed feedback linearization techniques for DC current regulation in MGs [25], as well as predictive-feedback linearization approaches [26], [27]. Unlike full linearization methods, some nonlinear control strategies preserve parts of the system's nonlinear structure, thereby enhancing closed-loop speed and stability. For example, the backstepping control method, grounded in Lyapunov stability theory, was proposed in [28] to control MGs while maintaining nonlinear terms. This technique combines backstepping, adaptive, and robust control principles to improve control performance under system uncertainties.

To further address the challenges of uncertain nonlinear systems, SMC has been widely adopted. SMC-based approaches have been developed for both AC microgrids [29] and hybrid AC–DC microgrids [30]. In [31], an SMC scheme was designed for an MG integrating a wind turbine, fuel cell, and solar array, while [32] examined standard SMC frameworks for MG regulation. A multifactorial SMC structure was introduced in [33]. However, as noted in [32] and [29], the use of linear sliding surfaces ensures only finite-time stability during the reaching phase, while the sliding phase remains asymptotically stable. To overcome this limitation, Terminal Sliding Mode Control was proposed in [32] for voltage regulation in MGs, guaranteeing finite-time stability in the sliding phase through nonlinear combinations of state variables in the sliding surface. Nevertheless, like [33], the first-order sliding mode approach leads to high-frequency oscillations in the control input, known as chattering, which complicates practical implementation. To mitigate chattering, a higher-order Super-Twisting Sliding Mode Control was combined with the backstepping technique in [35] for MG voltage regulation. Other strategies to alleviate chattering include the use of Fuzzy-Adaptive Sliding Mode Control, which was applied to MGs with energy storage systems in [36]. More recently, extended state observers have been employed to estimate system uncertainties and combined with SMC to suppress chattering, as demonstrated in [37] and [38]. However, these observer-based designs face challenges in proving finite-time stability under combined controller–observer dynamics. Another promising approach involves the integration of sliding mode control with fractional-order control theory, as presented in [39], to further reduce chattering effects. Additionally, the incorporation of adaptive estimation laws within SMC frameworks has emerged as a powerful method for uncertainty compensation without prior knowledge of the uncertainty bounds. This adaptive sliding mode approach was applied to MG control in [40], while [41] proposed adaptive estimation laws to effectively handle unknown system parameters. Table 1 qualitatively compares This paper with other references.

In this study, a nonlinear control strategy is proposed for voltage regulation in MGs. A SMC is developed to ensure robustness against system uncertainties. To achieve a continuous and smooth control signal, the second-order super-twisting sliding mode algorithm is employed. The proposed controller incorporates adaptive gain mechanisms to accurately estimate and compensate for uncertain system components. The finite-time stability of both the tracking and estimation errors is analytically demonstrated using the Lyapunov stability theorem. To this end, a nonlinear and uncertain mathematical model of the microgrid is first formulated. Subsequently, three different controllers—first-order sliding mode, super-twisting, and the proposed adaptive super-twisting controller—are individually designed for each subsection of the microgrid system. Finally, computer-based simulations are carried out to validate the performance of the proposed method, demonstrating its superior effectiveness and robustness compared to conventional control approaches.

Table 1. summary comparison of literature review

Ref	Controller	Adaptive	Chattering Reduction	Finite-Time Proof
[35]	ST-SMC	No	Yes	Partial
[36]	Fuzzy SMC	Yes	Moderate	No
[40]	Adaptive SMC	Yes	No	Yes
[41]	Adaptive SMC	Yes	Limited	Yes
Proposed	Adaptive	Yes	Strong	Yes

ST-SMC

The main contributions of this paper are summarized as follows:

1. A new adaptive super-twisting sliding mode controller (AST-SMC) is proposed for DC microgrid voltage regulation, in which both the reaching gain α and the discontinuous gain β are updated simultaneously via a Lyapunov-based estimation error signal. Unlike references [35]–[38], which adapt only the reaching gain, and references [39]–[41], which use fixed-gain ST-SMC, the dual adaptation ensures finite-time convergence without gain overestimation, thereby reducing chattering.
2. A formal finite-time convergence proof is provided (Appendix A), demonstrating that the adaptive gains satisfy $\dot{V} \le -\eta\sqrt{V}$, for all $t \ge 0$, guaranteeing sliding manifold reachability in finite time under bounded matched disturbances.
3. A comprehensive performance evaluation is conducted covering quantitative metrics (settling time, overshoot, RMSE) demonstrating robustness superior to benchmark controllers.

Note that this study focuses exclusively on islanded (off-grid) DC microgrid operation; extension to grid-connected scenarios, where the DC bus voltage is stiffened by the utility grid and the control objective shifts toward power flow regulation, is identified as a direction for future work.

2. Adaptive super-twisting control law

2.1. Sliding mode control

Consider a single input – single output uncertain nonlinear system [42]:

$$\dot{x} = f(x) + g(x)u + d(t) \tag{1}$$

where $x \in X \subset \mathbb{R}^n$ is a state vector, $u \in \mathbb{R}$ is the control input, $f(x) \in \mathbb{R}^n$ is a nonlinear function vector. Assume that:

A1. A sliding variable $s = s(x,t) \in \mathbb{R}$ is designed so that the system (1) desirable compensated dynamics are achieved in the sliding mode $s = s(x,t) = 0$.

A2. The relative degree of system (1) with the sliding variable $s(x,t)$ with respect to u equals one, and the internal dynamics are stable. Therefore, the sliding variable dynamics can be presented:

$$\begin{aligned}\dot{s} &= \frac{\partial s}{\partial t} + \frac{\partial s}{\partial x} f(x) + \frac{\partial s}{\partial t} g(x)u \\ &= a(x,t) + b(x,t)u\end{aligned} \tag{2}$$

A3. The function $b(x,t) \in \mathbb{R}$ is certain and the function $a(x,t) \in \mathbb{R}$ can be presented as:

$$a(x,t) = \bar{a}(x,t) + d \tag{3}$$

where $\bar{a}(x,t)$ and d are respectively known and uncertain parts of the $a(x,t)$.

In a DC microgrid, the lumped uncertainty d(t) encompasses unmodelled converter dynamics, cable resistance variations, and load fluctuations. All of these are bounded in practice: load power is limited by the rated capacity of connected devices, cable resistance varies within a small temperature-dependent range, and converter switching dynamics are bounded by the PWM saturation limits. Therefore, the assumption $|d(t)| \le D$ for some known constant $D > 0$ is physically justified. The time derivative of the disturbance is bounded because solar irradiance changes at a finite slew rate and battery state-of-charge dynamics evolve on a timescale of minutes to hours, not milliseconds. Load switching, while fast, produces step changes whose derivative can be treated as a bounded impulsive input within the discrete-time implementation. Both d(t) and ḋ(t) can be estimated via a disturbance observer or bounded using known converter ratings.

The bounded uncertainty assumption is physically justified because converter parameter variations, battery aging effects, and renewable generation fluctuations are inherently limited by the operating range of practical microgrid components. Similarly, the derivative of uncertainty remains bounded due to the finite dynamics of irradiance changes, load variations, and electrochemical processes within batteries. These quantities can be estimated using available measurements and observer-based techniques.

The problem is to design a smooth control u that drives the sliding variable s to zero in a finite time in the presence of the uncertainty d .

The classical first order sliding mode controller is able to stabilize the sliding variable. In classical SMC scheme, the control input is selected as follow:

$$u = \frac{1}{b(x,t)}\left[-\bar{a}(x,t) - k\,sign(s)\right] \tag{4}$$

where k is reaching term. Using $V = \frac{1}{2}s^2$ as a Lyapunov function candidate, a sufficient condition to guarantee the finite time stabilization of s is to ensure finite time stability condition [11]:

$$\dot{V} = s\dot{s} \le -\eta|s| \tag{5}$$

where η is a strictly positive constant, which implies that:

$$t_r \le \frac{|s(0)|}{\eta} \tag{6}$$

and t_r is the reaching time. The classical SM controller (4) contains the discontinuous nonlinear function $sign(s)$ with gain $k = L_d + \eta$. This nonlinearity can cause Chattering problem. Using continuous approximation method, the controller (4) is replaced by a continuous such as:

$$u = \frac{1}{b(x,t)}\left[-\bar{a}(x,t) - k\,sat_{\varepsilon}(s)\right] \tag{7}$$

In any case, this method reduces the accuracy of zeroing the sliding variable [43], [44].

2.2. Adaptive Super-Twisting Control Law

The sliding variable in (2) could also be stabilized at zero using second order super twisting control law [15]:

$$\begin{cases} u = \dfrac{1}{b(x,t)}\left[-\bar{a}(x,t) - k_1|s|^{1/2}sign(s) + w\right] \\ \dot{w} = -k_2 sign(s) \end{cases} \tag{8}$$

Using this controller, the sliding variable converges to zero, but the finite time stability of the sliding variable in this method is not proven according to Lyapunov theory and the convergence time relationship is not explicitly presented.

In this section, an Adaptive version of super twisting controller is introduced in the following Theorem.

Theorem 1: The modified form of the super-twisting second order sliding mode control:

$$\begin{cases} u = \dfrac{1}{b(x,t)}(-\bar{a}(x,t) - k_1|s|^{1/2}sign(s) \\ \quad + w - k_3\xi) \\ \dot{w} = -k_2 sign(s) \\ \dot{\xi} = k_2k_3|\xi|sign(s) - k_4 sign(\xi) \end{cases} \tag{9}$$

with conditions:

$$\begin{cases} k_1, k_2 > 0 \\ k_4 = L_g\left(L_d + |w|\right) + \eta \end{cases} \tag{10}$$

stabilizes system (2), and guarantees the convergence of the integral term $-w$ to the uncertainty $d(x,t)$ in a finite time. Parameters k_1, k_2, k_3 and η are positive constant. L_d and L_g are bounds of the uncertainty and its first derivative.

Proof:

Step 1 — Lyapunov function selection:

By controller (9) in system (2), we have closed-loop system dynamics:

$$\begin{cases} \dot{s} = -k_1|s|^{1/2}sign(s) - k_3\xi + d + w \\ \dot{w} = -k_2 sign(s) \\ \dot{\xi} = k_2k_3|\xi|sign(s) - k_4 sign(\xi) \end{cases} \tag{11}$$

By introducing the estimation error as $e = d(t) + w$, the closed-loop system dynamics can be rewritten:

$$\begin{cases} \dot{s} = -k_1|s|^{1/2}sign(s) - k_3\xi + e \\ \dot{e} = \dot{d} - k_2 sign(s) \\ \dot{\xi} = k_2k_3|\xi|sign(s) - k_4 sign(\xi) \end{cases} \tag{12}$$

Step 2 — Time derivative of V:

Now, consider the following Lyapunov function candidate:

$$V = k_2|s| + \frac{1}{2}e^2 + |\xi| \tag{13}$$

which is positive definite with $k_2 > 0$. By taking the time derivative of V , using (12), we obtain:

$$\begin{aligned} \dot{V} &= k_2\frac{s}{|s|}\dot{s} + e\dot{e} + \xi\dot{\xi} \\ &= k_2\frac{s}{|s|}\left(-k_1|s|^{1/2}sign(s) - k_3\xi + e\right) \\ &\quad + e\left(g(t) - k_2 sign(s)\right) \\ &\quad + \frac{\xi}{|\xi|}\left(k_2k_3|\xi|sign(s) - k_4 sign(\xi)\right) \\ &= -k_2k_1|s|^{1/2} - k_2\frac{s}{|s|}k_3\xi + k_2\frac{s}{|s|}e \\ &\quad + g(t)e - k_2 sign(s)e \\ &\quad + k_2k_3 sign(s)\xi - k_4 \\ &= -k_1k_2|s|^{1/2} + g(t)e - k_4 \end{aligned} \tag{14}$$

Step 3 — Finite-time convergence:

By choosing $k_1, k_2 > 0$ and $k_4 = L_g\left(L_d + |w|\right) + \eta$, where η is a strictly positive constant, yields:

$$\begin{aligned} \dot{V} &= -k_1 k_2 |s|^{1-\gamma} + g(t)\left(d + w\right) \\ &\quad - L_g\left(L_d + |w|\right) - \eta \le -\eta \end{aligned} \tag{15}$$

This condition that implies:

$$0 \le V\left(x(t)\right) = V\left(x(0)\right) - \eta t \tag{16}$$

and

$$t \le \frac{V\left(x(0)\right)}{\eta} \tag{17}$$

Condition (15) guarantees the finite time convergence of sliding variable and estimation error. Hence, the closed-loop system error converges in t that is the time of reaching $V\left(x(t)\right)$ to zero from an initial condition [45-47].

3. Dynamic model of the micro grid

Dynamic model of the micro grid is shown in **Fig. 1**. The DC microgrid considered in this study consists of four main subsystems: a PV) generation unit, a battery, a supercapacitor energy storage system, and a DC load connected through a common DC bus. The dynamic behavior of these subsystems is represented by Eqs. (18)–(22), which are derived from Kirchhoff's voltage and current laws and the averaged state-space model of DC/DC converters.

$$\begin{aligned} \dot{V}_{C_1} &= \frac{1}{R_1C_1}V_S - \frac{1}{R_1C_1}V_{C_1} - \frac{1}{C_1}I_{L_3} \\ \dot{V}_{C_2} &= \frac{1}{R_2C_2}V_{dc} - \frac{1}{R_2C_2}V_{C_2} + \frac{1}{C_2}I_{L_3}\left(1-u_1\right) \\ \dot{I}_{L_3} &= \frac{1}{L_3}V_{C_1} - \frac{1}{L_3}V_{C_2}\left(1-u_1\right) - \frac{R_{01}}{L_3}I_{L_3} \end{aligned} \tag{18}$$

Equation (18) describes the dynamics of the supercapacitor converter. The state variables include the inductor current and capacitor voltage associated with the supercapacitor branch. The control input u_1 represents the duty cycle of the corresponding DC/DC converter. This subsystem is mainly responsible for compensating fast transient power variations and maintaining short-term DC bus voltage stability.

$$\begin{aligned} \dot{V}_{C_4} &= \frac{1}{R_4C_4}V_B - \frac{1}{R_4C_4}V_{C_4} - \frac{1}{C_4}I_{L_6} \\ \dot{V}_{C_5} &= \frac{1}{R_5C_5}V_{dc} - \frac{1}{R_5C_5}V_{C_5} + \frac{1}{C_5}I_{L_6}\left(1-u_2\right) \\ \dot{I}_{L_6} &= \frac{1}{L_6}V_{C_4} - \frac{1}{L_6}V_{C_5}\left(1-u_2\right) - \frac{R_{04}}{L_6}I_{L_6} \end{aligned} \tag{19}$$

Equation (19) models the battery subsystem. The battery converter exchanges power with the DC bus through an inductor-capacitor network. The state variables represent the battery-side current and converter capacitor voltage, while the control signal (u_2) regulates the battery charging and discharging process. Due to its relatively slow dynamics, the battery mainly compensates low-frequency power fluctuations.

$$\begin{aligned} \dot{V}_{C_7} &= \frac{1}{R_7C_7}V_{PV} - \frac{1}{R_7C_7}V_{C_7} - \frac{1}{C_7}I_{L_9} \\ \dot{V}_{C_8} &= \frac{1}{R_8C_8}V_{dc} - \frac{1}{R_8C_8}V_{C_8} + \frac{1}{C_8}I_{L_9}\left(1-u_3\right) \\ \dot{I}_{L_9} &= \frac{1}{L_9}V_{C_7} - \frac{1}{L_9}V_{C_8}\left(1-u_3\right) - \frac{R_{08}}{L_9}I_{L_9} \\ &\quad + \frac{1}{L_9}\left(R_{08} - R_{07}\right)I_{L_9}u_3 \end{aligned} \tag{20}$$

Equation (20) represents the photovoltaic subsystem. The inductor current and capacitor voltage of the PV converter are selected as state variables. The control input (u_3) determines the converter duty ratio and enables the PV current to track its reference generated by the maximum power point tracking (MPPT) algorithm. Consequently, this subsystem regulates renewable power injection into the DC microgrid.

$$\begin{aligned} \dot{V}_{C_{11}} &= \frac{1}{R_{11}C_{11}}V_L - \frac{1}{R_{11}C_{11}}V_{C_{11}} - \frac{1}{C_{11}}I_{L_{13}} \\ \dot{V}_{C_{12}} &= \frac{1}{R_{12}C_{12}}V_{dc} - \frac{1}{R_{12}C_{12}}V_{C_{12}} + \frac{1}{C_{12}}I_{L_{13}}u_4 \\ \dot{I}_{L_{13}} &= \frac{1}{L_{13}}V_{C_{11}} + V_{C_{12}}u_4 - \frac{R_{011}}{L_{13}}I_{L_{13}} \\ &\quad + \frac{1}{L_{13}}\left(R_{012} - R_{011}\right)I_{L_{13}}u_4 \end{aligned} \tag{21}$$

Equation (21) describes the load-side converter dynamics. The output voltage supplied to the DC load is controlled through the converter duty cycle (u_4). This subsystem ensures that the load voltage remains close to its desired reference despite disturbances and load variations.

$$\begin{aligned} \dot{V}_{dc} &= \frac{1}{C_{10}}\Big[\frac{1}{R_2}\left(V_{C_2} - V_{dc}\right) + \frac{1}{R_5}\left(V_{C_5} - V_{dc}\right) \\ &\quad + \frac{1}{R_8}\left(V_{C_8} - V_{dc}\right) + \frac{1}{R_{12}}\left(V_{C_{12}} - V_{dc}\right)\Big] \end{aligned} \tag{22}$$

Finally, Equation (22) represents the DC-link voltage dynamics, which constitute the main controlled variable of the microgrid. According to the capacitor current balance principle, the DC-link voltage is influenced by the power exchange among the PV array, battery, supercapacitor, and load subsystems. Therefore, maintaining a stable DC-link voltage requires coordinated control of all converter units.

The model parameters have the following physical meanings: (L_i) and (C_i) denote the inductances and capacitances of the converter filters, respectively; (R_i) represents the equivalent parasitic resistances; (V_{dc}) is the DC bus voltage; (I_L) denotes the inductor current; (u_i) corresponds to the converter duty cycle; and (d_i) represents lumped uncertainties arising from parameter variations, unmodeled dynamics, and external disturbances. These uncertainties include battery degradation effects, converter losses, load fluctuations, and variations in solar irradiance.

The dynamic model adopted in this paper is based on the averaged converter modeling approach commonly employed in DC microgrid studies and provides a suitable framework for designing robust nonlinear controllers under parametric uncertainties and external disturbances.

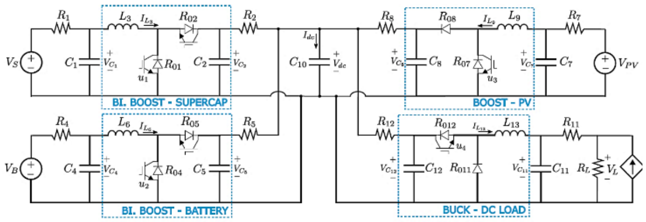

Fig. 1. Electrical micro grid scheme

Also, the complete operation of the proposed AST-SMC is illustrated in **Fig. 2**. The algorithm proceeds as follows:

(Step 1) Measure the DC bus voltage V_{dc} and inductor current i_L.

(Step 2) Compute the sliding surface.

(Step 3) Update the adaptive gains $\alpha(t)$ and $\beta(t)$ using the adaptive law based on the current value of s.

(Step 4) Compute the super-twisting control input u.

(Step 5) Apply u to the PWM modulator of the DC/DC converter.

The cycle repeats at each sampling instant $T_s = 1/f_{sw}$.

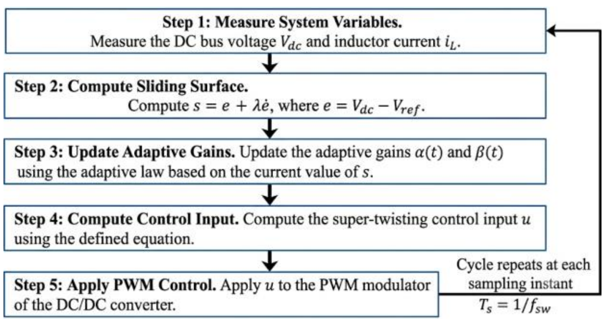

Fig. 2. The proposed models flowchart.

4. Controller design

In this section, first-order sliding mode, super twisting and adaptive super twisting methods are designed separately for all four micro grid subsections.

4.1. Control of super-capacitor subsystem

Super capacitor is considered to regulate V_{dc} and this is done by controlling V_{C2} in the related convertor. C_2 is utilized for damping transient oscillation in the grid. So, u_1 is designed such that V_{C2^*} is tracked by V_{C2}. For this purpose, Eq. (18) can be rewritten in the following form:

$$\dot{V}_{C_2} = \frac{1}{R_2C_2}V_{dc} - \frac{1}{R_2C_2}V_{C_2} + \frac{I_{L_3}}{C_2} - \frac{I_{L_3}}{C_2}u_1 + d_1 \qquad (23)$$
$$y_1 = V_{C_2}$$

where $y_1 = V_{C_2}$ is the first output, and d_1 is sum of parametric model uncertainty. To design controllers, sliding variables is defined as below:

$$s_1 = y_1 - y_{1d} = V_{C_2} - V_{C_2}^{*} \qquad (24)$$

Also, the dynamic of the sliding variable is calculated by Eq. (25):

$$\dot{s}_1 = \dot{V}_{C_2} - \dot{V}_{C_2}^{*}$$
$$= \frac{1}{R_2C_2}V_{dc} - \frac{1}{R_2C_2}V_{C_2} + \frac{I_{L_3}}{C_2} - \frac{I_{L_3}}{C_2}u_1 + d_1 - \dot{V}_{C_2}^{*} \qquad (25)$$

The first order sliding mode controller for super-capacitor subsystem is then designed as follows:

$$u_1 = \frac{C_2}{I_{L_3}}\Big(-\frac{1}{R_2C_2}V_{dc} + \frac{1}{R_2C_2}V_{C_2} - \frac{I_{L_3}}{C_2} - \dot{V}_{C_2}^{*} + k_1 sign(s_1)\Big) \qquad (26)$$
$$k_1 = L_{d_1} + \eta_1$$

Using super-twisting sliding mode control theory, controller input is sketched by Eq. (27) for super-capacitor subsystem.

$$u_1 = \frac{C_2}{I_{L_3}}\Big(-\frac{1}{R_2C_2}V_{dc} + \frac{1}{R_2C_2}V_{C_2} - \frac{I_{L_3}}{C_2} - \dot{V}_{C_2}^{*} + k_{11}|s_1|^{1/2} sign(s_1) - w_1\Big) \qquad (27)$$
$$\dot{w}_1 = -k_{12} sign(s_1)$$

Finally, proposed adaptive super twisting controller is designed as follow:

$$u_1 = \frac{C_2}{I_{L_3}}\Big(-\frac{1}{R_2C_2}V_{dc} + \frac{1}{R_2C_2}V_{C_2} - \frac{I_{L_3}}{C_2} - \dot{V}_{C_2}^{*} + k_{11}|s_1|^{1/2} sign(s_1) - w_1 + k_{13}\xi_1\Big) \qquad (28)$$
$$\dot{w}_1 = -k_{12} sign(s_1)$$
$$\dot{\xi}_1 = k_{12}k_{13}|\xi_1| sign(s_1) - k_{14} sign(\xi_1)$$

where gains are chosen by Eq. (29):

$$\begin{cases} k_{11}, k_{12} > 0 \\ k_{14} = L_{g_1}\left(L_{d_1} + |w_1|\right) + \eta_1 \end{cases} \qquad (29)$$

Parameters k_{11}, k_{12}, k_{13} and η_1 are positive constant, L_{d_1} and L_{g_1} are bounds of the uncertainty and its first derivative.

4.2. Battery subsystem control

I_L^* is the reference signal for current of battery which is determined by the second order controller to control low frequencies in the micro grids. u_2 control law is designed in the way that I_L tracks I_L^*.

$$\dot{I}_{L_6} = \frac{1}{L_6}V_{C_4} - \frac{1}{L_6}V_{C_5} - \frac{R_{04}}{L_6}I_{L_6} + \frac{V_{C_5}}{L_6}u_2 + d_2 \qquad (30)$$
$$y_2 = I_{L_6}$$

where $y_2 = I_{L_6}$ is the output, and d_2 is uncertainty in this subsystem. To design controller for battery subsystem, sliding variable is defined as Eq. (31) according to tracking error.

$$s_2 = y_2 - y_{2d} = I_{L_6} - I_{L_6}^{*} \qquad (31)$$

The dynamic of this sliding variable is calculated by Eq. (32):

$$\dot{s}_2 = \dot{I}_{L_6} - \dot{I}_{L_6}^{\ *} = \frac{1}{L_6}V_{C_4} - \frac{1}{L_6}V_{C_5} - \frac{R_{04}}{L_6}I_{L_6} + \frac{V_{C_5}}{L_6}u_2 + d_2 - \dot{I}_{L_6}^{\ *} \quad (32)$$

The first order sliding mode controller for battery subsystem is then designed as follows:

$$u_2 = \frac{L_6}{V_{C_5}}(-\frac{1}{L_6}V_{C_4} + \frac{1}{L_6}V_{C_5} + \frac{R_{04}}{L_6}I_{L_6} + \dot{I}_{L_6}^{\ *} - k_2 sign(s_2)), \quad (33)$$
$$k_2 = L_{d_2} + \eta_2$$

Using super-twisting sliding mode control theory, controller input is sketched by Eq. (34) for battery subsystem.

$$u_2 = \frac{L_6}{V_{C_5}}(-\frac{1}{L_6}V_{C_4} + \frac{1}{L_6}V_{C_5} + \frac{R_{04}}{L_6}I_{L_6} + \dot{I}_{L_6}^{\ *} - k_{21}|s_2|^{1/2} sign(s_2) + w_2) \quad (34)$$
$$\dot{w}_2 = -k_{22} sign(s_2)$$

and proposed adaptive super twisting controller is designed as follow for battery subsystem:

$$u_2 = \frac{L_6}{V_{C_5}}(-\frac{1}{L_6}V_{C_4} + \frac{1}{L_6}V_{C_5} + \frac{R_{04}}{L_6}I_{L_6} + \dot{I}_{L_6}^{\ *} - k_{21}|s_2|^{1/2} sign(s_2) + w_2 - k_{23}\xi_2) \quad (35)$$
$$\dot{w}_2 = -k_{22} sign(s_2)$$
$$\dot{\xi}_2 = k_{22}k_{23}|\xi_2| sign(s_2) - k_{24} sign(\xi_2)$$

Gains can be selected by Eq. (36):

$$\begin{cases} k_{21}, k_{22} > 0 \\ k_{24} = L_{g_2}\left(L_{d_2} + |w_2|\right) + \eta_2 \end{cases} \quad (36)$$

Parameters k_{21}, k_{22}, k_{23} and η_2 are positive and constant, L_{d_2} and L_{g_2} are bounds of the uncertainty and its first derivative in battery subsystem.

4.3. Controller for PV part

$I_{L_9}^{\ *}$, the reference current signal of PV, is calculated by tracking algorithm. The main purpose in this section will be tracking $I_{L_9}^{\ *}$; therefore, u_3 control law is designed in the way that I_{L9} tracks I_{L9}*.

$$\dot{I}_{L_9} = \frac{1}{L_9}V_{C_7} - \frac{1}{L_9}V_{C_8} - \frac{R_{08}}{L_9}I_{L_9} + \frac{1}{L_9}\left(\left(R_{08} - R_{07}\right)I_{L_9} + V_{C_8}\right)u_3 + d_3 \quad (37)$$
$$y_3 = I_{L_9}$$

where $y_3 = I_{L9}$ is the third output, and d_3 is sum of parametric and model uncertainty in this subsystem. To design sliding mode controller for this subsystem, sliding variable is defined as Eq. (38) according to tracking error.

$$s_3 = y_3 - y_{3d} = I_{L9} - I_{L9}^{\ *} \quad (38)$$

The third sliding variable dynamic equation is calculated by Eq. (39):

$$\dot{s}_2 = \dot{I}_{L_9} - \dot{I}_{L_9}^{\ *} = \frac{1}{L_9}V_{C_7} - \frac{1}{L_9}V_{C_8} - \frac{R_{08}}{L_9}I_{L_9} + \frac{1}{L_9}\left(\left(R_{08} - R_{07}\right)I_{L_9} + V_{C_8}\right)u_3 + d_3 - \dot{I}_{L_9}^{\ *} \quad (39)$$

Then first order sliding mode, super twisting and adaptive super twisting sliding mode controllers are designed as relations (40) to (43) for the PV subsystem:

$$u_3 = \frac{L_9}{\left(R_{08} - R_{07}\right)I_{L_9} + V_{C_8}}(-\frac{1}{L_9}V_{C_7} + \frac{1}{L_9}V_{C_8} + \frac{R_{08}}{L_9}I_{L_9} + \dot{I}_{L_9}^{\ *} - k_3 sign(s_3)), \quad (40)$$
$$k_3 = L_{d_3} + \eta_3$$

$$u_3 = \frac{L_9}{\left(R_{08} - R_{07}\right)I_{L_9} + V_{C_8}}(-\frac{1}{L_9}V_{C_7} + \frac{1}{L_9}V_{C_8} + \frac{R_{08}}{L_9}I_{L_9} + \dot{I}_{L_9}^{\ *} - k_{31}|s_3|^{1/2} sign(s_3) + w_3) \quad (41)$$
$$\dot{w}_3 = -k_{32} sign(s_3)$$

$$u_3 = \frac{L_9}{\left(R_{08} - R_{07}\right)I_{L_9} + V_{C_8}}(-\frac{1}{L_9}V_{C_7} + \frac{1}{L_9}V_{C_8} + \frac{R_{08}}{L_9}I_{L_9} + \dot{I}_{L_9}^{\ *} - k_{31}|s_3|^{1/2} sign(s_3) + w_3 - k_{33}\xi_3) \quad (42)$$
$$\dot{w}_3 = -k_{32} sign(s_3)$$
$$\dot{\xi}_3 = k_{32}k_{33}|\xi_3| sign(s_3) - k_{34} sign(\xi_3)$$

Gains can be selected by Eq. (43):

$$\begin{cases} k_{31}, k_{32} > 0 \\ k_{34} = L_{g_3}\left(L_{d_3} + |w_3|\right) + \eta_3 \end{cases} \quad (43)$$

Parameters k_{31}, k_{32}, k_{33} and η_3 are positive and constant, L_{d_3} and L_{g_3} are bounds of the uncertainty and its first derivative.

4.4. DC load subsystem controlling

DC load must be fed by a constant voltage. Reference signal $V_{C_{11}}^{\ *}$ is appointed by the gird's standards. The main goal is tracking the voltage. To achieve this, u_4 voltage law must be designed in the way which $V_{C_{11}}$ tracks $V_{C_{11}}^*$; therefore, Equations (23) are rewritten as Equation (44).

$$\begin{aligned} \dot{V}_{C_{11}} &= \frac{1}{R_{11}C_{11}}V_L - \frac{1}{R_{11}C_{11}}V_{C_{11}} - \frac{1}{C_{11}}I_{L_{13}} \\ \dot{I}_{L_{13}} &= \frac{1}{L_{13}}V_{C_{11}} - \frac{R_{011}}{L_{13}}I_{L_{13}} \\ &+\left(\frac{1}{L_{13}}(R_{012}-R_{011})I_{L_{13}} + V_{C_{12}}\right)u_4 + d_4 \\ y_4 &= V_{C_{11}} \end{aligned} \tag{44}$$

where $y_4 = V_{C_{11}}$ is the fourth output, and d_4 is sum of parametric and model uncertainty in this subsystem. To design the sliding mode controller for this subsystem, the sliding variable is defined as Equation 45 according to tracking error.

$$\begin{aligned} s_4 &= (\dot{y}_3 - \dot{y}_{3d}) + \lambda(y_3 - y_{3d}) \\ &= (\dot{V}_{C_{11}} - \dot{V}_{C_{11}}^*) + \lambda(V_{C_{11}} - V_{C_{11}}^*) \end{aligned} \tag{45}$$

The dynamic equation of the fourth sliding variable is calculated by Equation (46):

$$\begin{aligned} \dot{s}_2 &= (\ddot{V}_{C_{11}} - \ddot{V}_{C_{11}}^*) + \lambda(\dot{V}_{C_{11}} - \dot{V}_{C_{11}}^*) \\ &= \frac{1}{R_{11}C_{11}}\dot{V}_L - \frac{1}{R_{11}C_{11}}\dot{V}_{C_{11}} \\ &- \frac{1}{C_{11}}\left(\frac{1}{L_{13}}V_{C_{11}} - \frac{R_{011}}{L_{13}}I_{L_{13}}\right) - \ddot{V}_{C_{11}}^* + \lambda(\dot{V}_{C_{11}} - \dot{V}_{C_{11}}^*) \\ &- \frac{1}{C_{11}}\left(\frac{1}{L_{13}}(R_{012}-R_{011})I_{L_{13}} + V_{C_{12}}\right)u_4 - \frac{1}{C_{11}}d_4 \\ &= f_4 + g_4 u_4 + d_4' \end{aligned} \tag{46}$$

Finally, first order sliding mode, super twisting and adaptive super twisting sliding mode controllers are designed as relations (47) to (50) for the DC load subsystem:

$$\begin{aligned} u_4 &= \frac{1}{g_4}[f_4 - k_4 sign(s_4)] \\ k_4 &= L_{d_4'} + \eta_4 \end{aligned} \tag{47}$$

$$\begin{aligned} u_4 &= \frac{1}{g_4}\left[f_4 - k_{41}|s_4|^{1/2} sign(s_4) + w_4\right] \\ \dot{w}_4 &= -k_{42} sign(s_4) \end{aligned} \tag{48}$$

$$\begin{aligned} u_4 &= \frac{1}{g_4}(f_4 - k_{41}|s_4|^{1/2} sign(s_4) \\ &+ w_4 - k_{43}\xi_4)) \\ \dot{w}_4 &= -k_{42} sign(s_4) \\ \dot{\xi}_4 &= k_{42}k_{43}|\xi_4| sign(s_4) - k_{44} sign(\xi_4) \end{aligned} \tag{49}$$

Gains can be selected by Eq. (50):

$$\begin{cases} k_{41}, k_{42} > 0 \\ k_{44} = L_{g_4}\left(L_{d_4} + |w_4|\right) + \eta_4 \end{cases} \tag{50}$$

Parameters k_{41}, k_{42}, k_{43} and η_4 are positive and constant, L_{d_4} and L_{g_4} are bounds of the uncertainty d_4 and its first derivative $\dot{d}_4 = g_4$.

4.5. Real-Time Implementation Considerations

The computational burden of the proposed AST-SMC is assessed to verify its feasibility for real-time embedded implementation. The per-sample operations required are:

(i) Sliding surface computation: 1 subtraction, 1 multiplication, 1 differentiation ≈ 3 FLOPs

(ii) Control law: 1 absolute value, 1 square root, 2 multiplications ≈ 5 FLOPs

(iii) Adaptive law: 2 integrations, 2 multiplications ≈ 4 FLOPs

Total computational cost: approximately 12 FLOPs per control cycle.

For a Texas Instruments TMS320F28335 DSP (150 MHz, single-cycle multiply-accumulate), the estimated execution time at a 10 kHz switching frequency ($T_s = 100\,\mu s$) is approximately 0.08 µs per cycle, which represents less than 0.1% of the available computational budget. This leaves sufficient margin for communication, protection, and supervisory tasks.

The following practical issues must be considered for hardware deployment:

(a) Minimum PWM pulse width: The control output u must be constrained to avoid generating pulses shorter than the converter's minimum on-time (typically 200 ns for MOSFETs). A saturation block should be included before the PWM modulator.

(b) Measurement noise: Anti-aliasing low-pass filters with cutoff frequency $f_{sw}/10$ should be applied to voltage and current sensor signals prior to computing the sliding surface s.

(c) Discretization of adaptive law: The continuous-time adaptive law is implemented using forward Euler discretization: $\alpha[k+1] = \alpha[k] + k_1 \mid s[k] \mid T_s$

The sampling interval T_s must satisfy: $T_s < \frac{1}{2 \cdot BW_{adaptive}}$ to ensure stability.

(d) Dead-band compensation: Gate dead-band in half-bridge switches introduces a voltage error proportional to dead-time t_d and switching frequency f_{sw}. This effect should be compensated by adding: $V_{comp} = t_d \cdot f_{sw} \cdot V_{bus}$ to the control output.

5. Simulation results

In this section, the simulation results for three control schemes—namely, the conventional first-order SMC, the super-twisting controller, and the adaptive super-twisting controller—are presented. The microgrid parameters utilized in the simulations are adopted from [48].

The load current variation is illustrated in **Fig. 3**, while **Fig. 4** depicts the voltage variations of the battery, supercapacitor, and connected PV unit. Furthermore, the voltage responses of capacitors C1, C4, and C7 are shown in **Fig. 5**.

Fig. 6 illustrates the voltage response of capacitor (C_{11}) under the action of the conventional Sliding Mode Controller, the standard Super-Twisting controller, and the proposed AST-SMC applied to the four converters of the DC microgrid. The figure demonstrates the ability of each control strategy to regulate the capacitor voltage and track the reference value (V_{C11}^{*}) under the considered operating conditions.

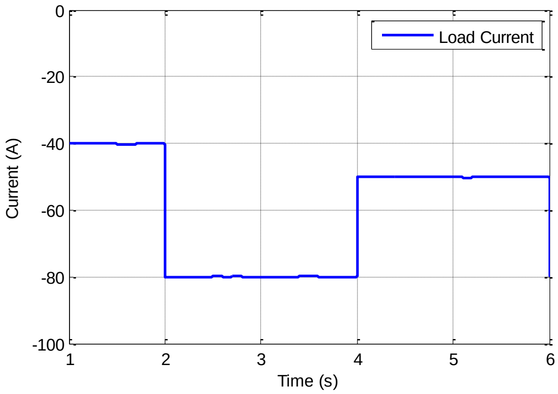

Fig. 3. Load current variation

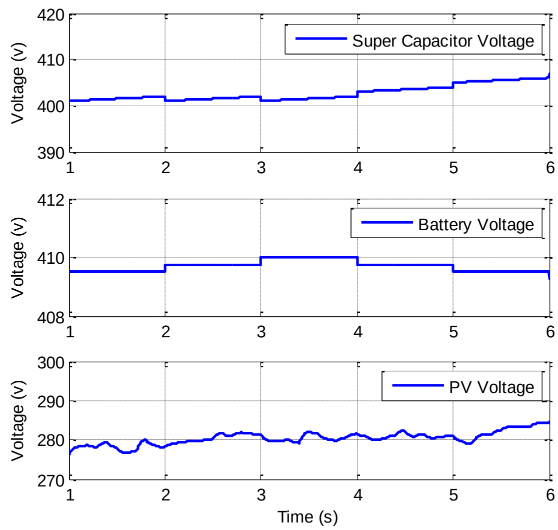

Fig. 4. Voltage variation of battery, super capacitor and connected PV

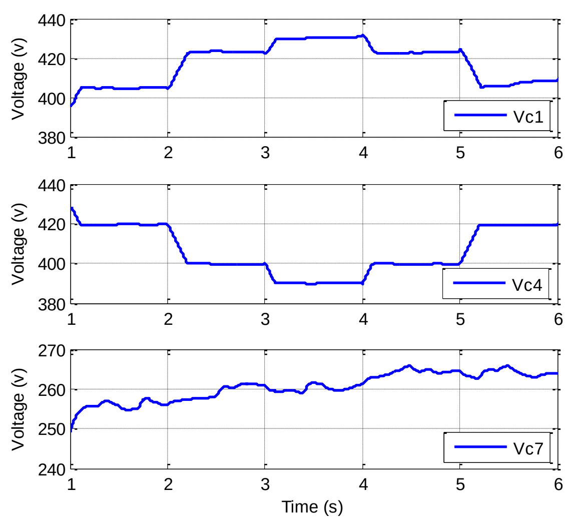

Fig. 5. Voltage variation of C1, C4, C7

As can be observed, all controllers are capable of driving the system states toward the desired operating point; however, significant differences exist in their transient and steady-state performances. The conventional SMC exhibits noticeable oscillations around the reference voltage due to the well-known chattering phenomenon, which results in increased voltage fluctuations and a longer settling period. Although the standard ST controller effectively reduces chattering compared with the conventional SMC, small tracking deviations and residual oscillations are still observed during transient conditions.

In contrast, the proposed AST-SMC achieves the fastest convergence to the reference voltage while maintaining a smooth control action. The adaptive gain mechanism dynamically adjusts the controller parameters according to the instantaneous tracking error and system uncertainties, allowing the controller to provide strong corrective action during large disturbances and reduced control effort near the equilibrium point. Consequently, the voltage (V_{C11}) reaches its reference value with a shorter settling time, lower overshoot, and significantly reduced steady-state error compared with the benchmark controllers.

Furthermore, the results indicate that the proposed controller maintains excellent voltage regulation despite the nonlinear behavior and parameter uncertainties inherent in the microgrid components. The reduction in oscillatory behavior demonstrates the effectiveness of the adaptive super-twisting algorithm in mitigating chattering while preserving the robustness properties of sliding mode control. Overall, the superior tracking accuracy and dynamic performance achieved by the AST-SMC confirm its suitability for high-performance voltage regulation in DC microgrid applications.

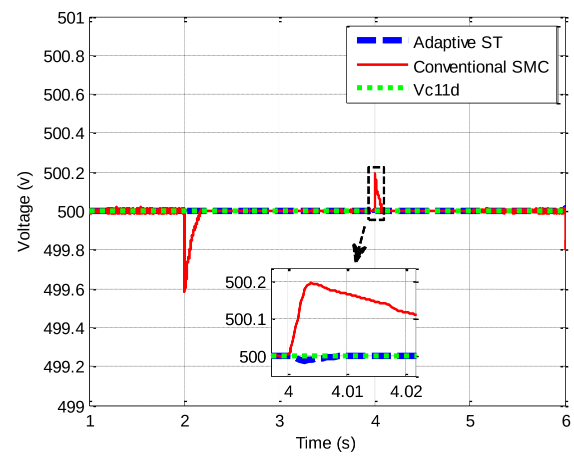

Fig. 6. Voltage variation of C_{11} and desired voltage V_{C11}* by applying conventional SMC and adaptive ST sliding mode controllers

Fig. 7–10 present the dynamic responses of the inductor currents (I_{L3}), (I_{L6}), (I_{L9}), and (I_{L13}) under the conventional Sliding Mode Controller, the standard Super-Twisting controller, and the proposed AST-SMC. These currents play a critical role in power transfer and energy management within the DC microgrid, making their accurate regulation essential for maintaining overall system stability and performance.

As observed in Fig. 7–10, the proposed AST-SMC provides significantly smoother current trajectories than the conventional SMC. While the conventional SMC successfully regulates the inductor currents, the switching nature of its discontinuous control law introduces high-frequency oscillations and chattering, which are clearly reflected in the current waveforms. Such oscillations may increase power losses, accelerate component aging, and adversely affect the reliability of power electronic converters in practical implementations. The standard ST controller partially alleviates these oscillations by employing a higher-order sliding mode strategy. Nevertheless, transient fluctuations and minor oscillatory behavior remain present, particularly during rapid changes in operating conditions. In contrast, the proposed AST-SMC exhibits smoother current responses with substantially reduced ripple and improved transient characteristics. This improvement is mainly attributed to the adaptive adjustment of the super-twisting gains, which enables the controller to continuously balance robustness and control smoothness according to the system's instantaneous operating conditions. Moreover, the current responses obtained with the AST-SMC demonstrate faster convergence to their reference values and enhanced disturbance rejection capability. Following transient events, the currents quickly return to their desired trajectories with minimal overshoot and negligible steady-state error. The reduced current ripple also contributes to lower electromagnetic stress on converter components and improved power quality throughout the microgrid. Overall, the results presented in Fig. 7–10 confirm that the proposed AST-SMC not only preserves the robustness advantages of sliding mode control but also significantly improves current regulation performance by reducing chattering, minimizing oscillations, and enhancing tracking accuracy. These characteristics make the proposed controller particularly attractive for practical DC microgrid applications where smooth current regulation and converter reliability are of paramount importance.

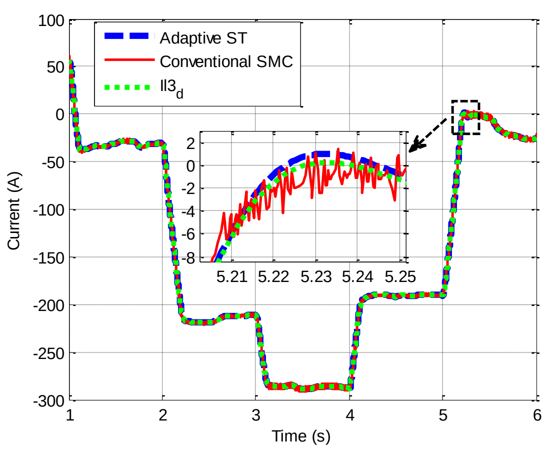

Fig. 7. Current variation of I_{L3} and desired voltage I_{L3}* by applying conventional SMC and adaptive ST sliding mode controllers

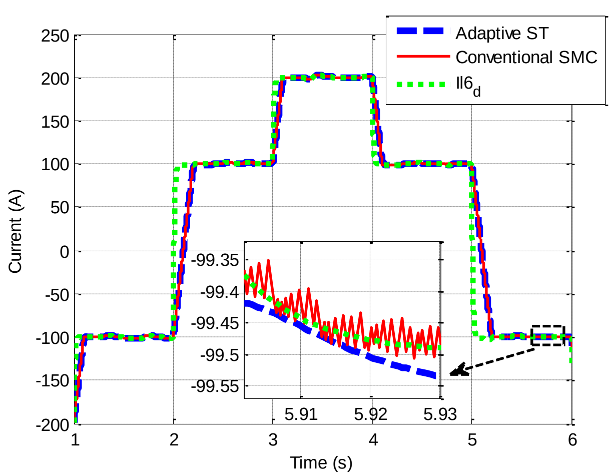

Fig. 8. Current variation of IL6 and desired voltage IL6* by applying conventional SMC and adaptive ST sliding mode controllers

Voltage variation of capacitor C_2 is shown in **Fig. 11**. It can be seen that both controllers have good tracking but voltage variation in the conventional SMC is not completely smooth.

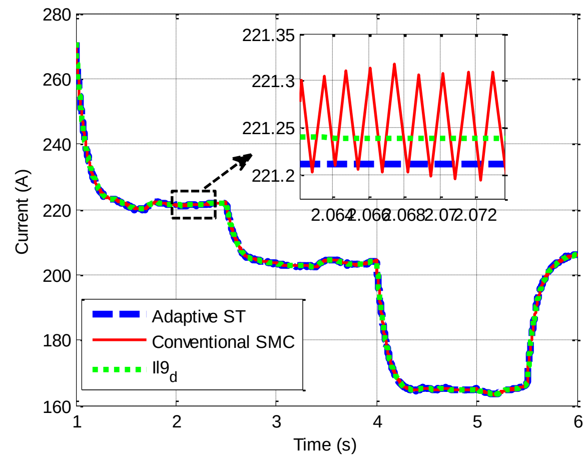

Fig. 9. Current variation of I_{L9} and desired voltage I_{L9}* by applying conventional SMC and adaptive ST sliding mode controllers

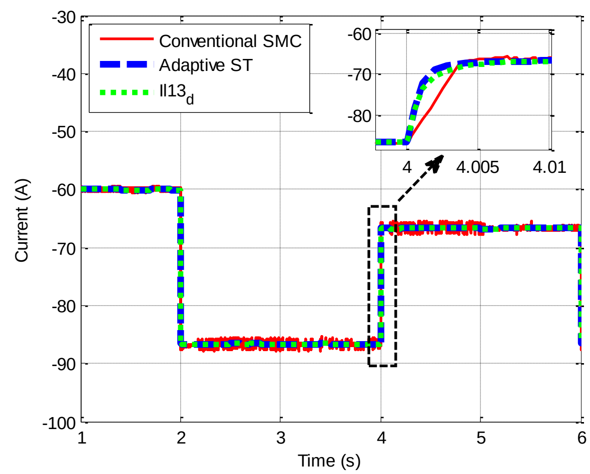

Fig. 10. Current variation of I_{L13} and desired voltage I_{L13}* by applying conventional SMC and adaptive ST sliding mode controllers

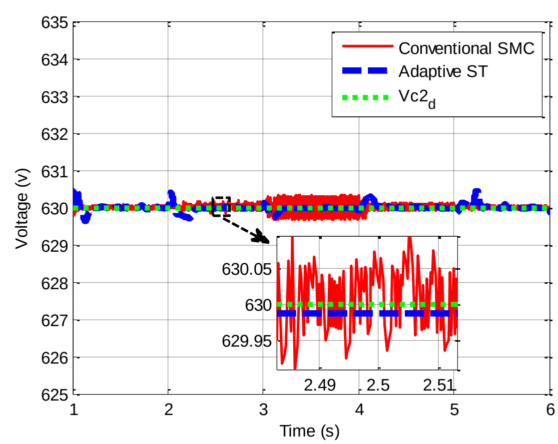

Fig. 11. Voltage variation V_{C2} and desired voltage V_{C2}* by applying conventional SMC and adaptive ST sliding mode controllers

As shown in **Fig. 12**, DC voltage is less than %5 by applying both control methods. Finally, as shown in **Fig. 13**, proposed method has smoother control signals in comparison with conventional SMC method.

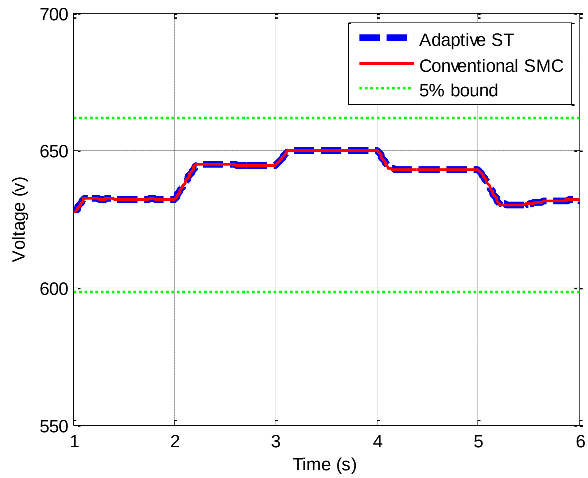

Fig. 12. Voltage variation of DC Link by applying conventional SMC and adaptive ST sliding mode controllers

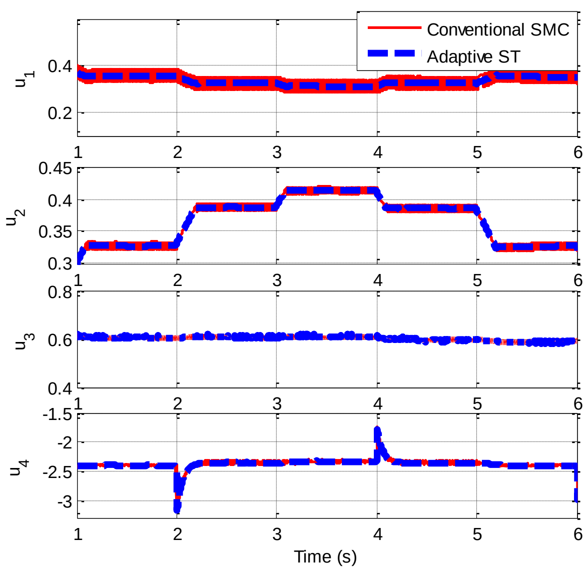

Fig. 13. Control inputs variations by applying conventional SMC and adaptive ST sliding mode controllers

Fig. 14 illustrates the voltage response of capacitor (C_{11}) when the standard ST controller and the proposed AST-SMC are applied to the four converters of the DC microgrid. The figure compares the ability of both controllers to regulate the capacitor voltage and accurately track the desired reference value (V_{C11}^{*}). As shown in the figure, both control strategies are capable of stabilizing the system and driving the capacitor voltage toward its reference value. However, the proposed AST-SMC exhibits noticeably superior dynamic performance. The voltage response under the AST-SMC reaches the desired operating point more rapidly, with a shorter settling time and reduced transient deviations compared with the standard ST controller. This behavior indicates that the adaptive gain mechanism enables the controller to react more effectively to system nonlinearities, parameter uncertainties, and external disturbances. Furthermore, the tracking accuracy achieved by the AST-SMC is higher than that of the conventional ST controller. The voltage trajectory remains closer to the reference signal throughout both transient and steady-state operating conditions, resulting in a smaller tracking error and improved voltage regulation quality. In addition, the adaptive adjustment of the super-twisting gains allows the controller to maintain high robustness without requiring excessively conservative gain values, thereby improving control efficiency and reducing unnecessary control activity. Another important observation is the smoother voltage response obtained with the AST-SMC. The adaptive controller effectively suppresses residual oscillations that may still be present in the standard ST response, leading to enhanced system stability and improved power quality. Such improvements are particularly important in DC microgrid applications, where precise voltage regulation is essential for the reliable operation of distributed energy resources, energy storage systems, and sensitive loads. Overall, the results presented in Fig. 14 demonstrate that the proposed AST-SMC provides faster convergence, higher tracking accuracy, better disturbance rejection capability, and smoother voltage regulation than the standard ST controller, confirming the effectiveness of the proposed adaptive control strategy for DC microgrid applications.

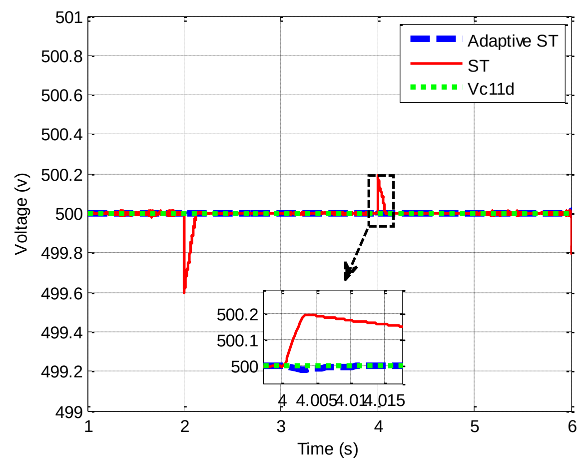

Fig. 14. Voltage variation of C_{11} and desired voltage V_{C11}* by applying adaptive ST and super twisting sliding mode controllers

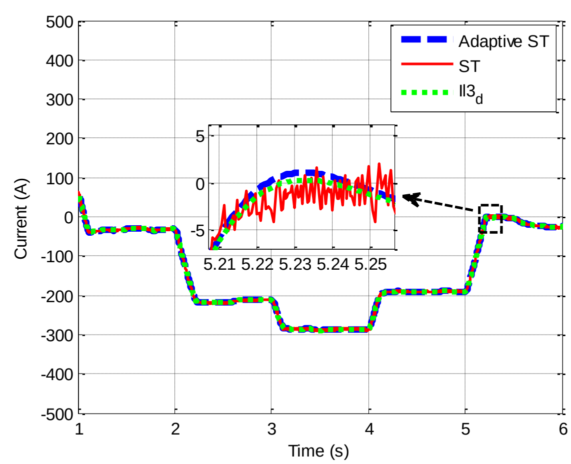

Fig. 15. Current variation of I_{L3} and desired voltage I_{L3}* by applying adaptive ST and super twisting sliding mode controllers

Furthermore, as shown in **Fig. 15** to **Fig. 18**, currents of L_3, L_6, L_9 and L_{13} have good tracking, but signals in proposed controller have smoother behavior in comparison with ST method.

Fig. 19 and 20 present the voltage responses of capacitors (C_5), (C_8), (C_{12}), and (C_2), where (C_2) is regulated to track the reference voltage (V_{C2}^{*}). These figures compare the performance of the standard ST controller and the proposed AST-SMC in regulating the capacitor voltages under the considered operating conditions. As shown in the figures, both controllers successfully achieve voltage regulation and maintain the capacitor voltages close to their desired reference values. The responses demonstrate the inherent robustness of higher-order sliding mode control techniques, enabling accurate tracking despite the nonlinear dynamics and parameter uncertainties present in the DC microgrid. Consequently, both methods exhibit satisfactory steady-state performance with relatively small tracking errors. However, a closer examination of the transient and steady-state responses reveals noticeable differences between the two controllers. Although the ST controller provides acceptable voltage regulation, its output signals are not completely smooth and exhibit small oscillations around the reference values. These residual fluctuations are particularly evident during transient intervals and after operating-point changes, indicating the presence of remaining chattering effects and imperfect disturbance compensation. In contrast, the proposed AST-SMC generates significantly smoother voltage trajectories. The adaptive gain mechanism continuously adjusts the controller parameters according to the system conditions, allowing the controller to apply only the level of corrective action required to maintain stability and tracking performance. As a result, voltage oscillations are substantially reduced, yielding smoother transient behavior, improved damping characteristics, and enhanced steady-state regulation. Furthermore, the AST-SMC demonstrates faster convergence to the desired operating point and improved disturbance rejection capability.

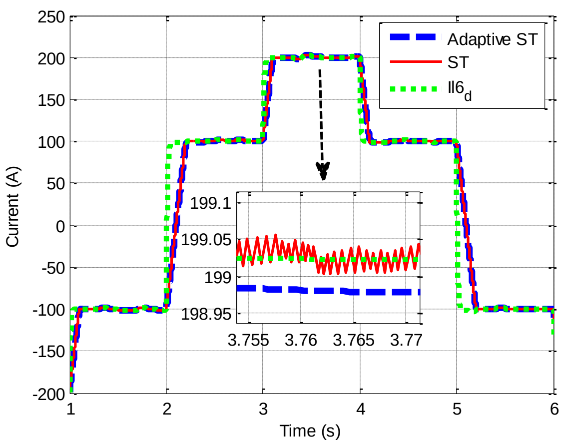

Fig. 16. Current variation of I_{L6} and desired voltage I_{L6}* by applying adaptive ST and super twisting sliding mode controllers

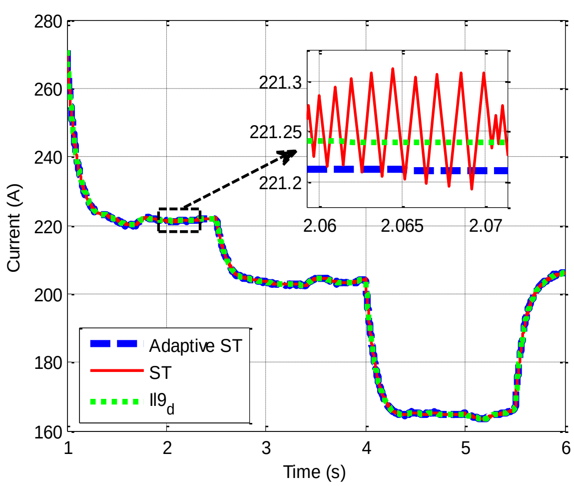

Fig. 17. Current variation of I_{L9} and desired voltage I_{L9}* by applying adaptive ST and super twisting sliding mode controllers

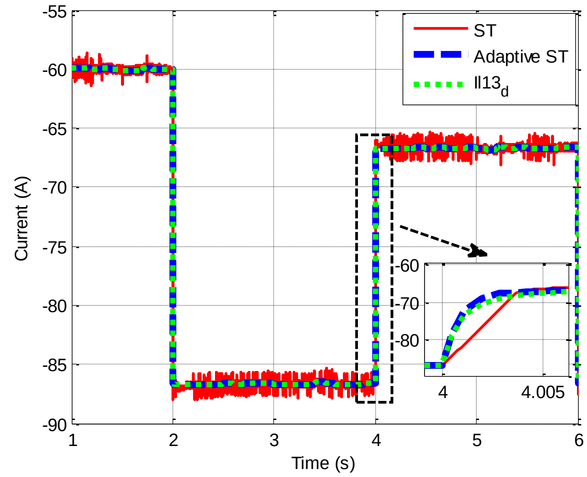

Fig. 18. Current variation of I_{L13} and desired voltage I_{L13}* by applying adaptive ST and super twisting sliding mode controllers

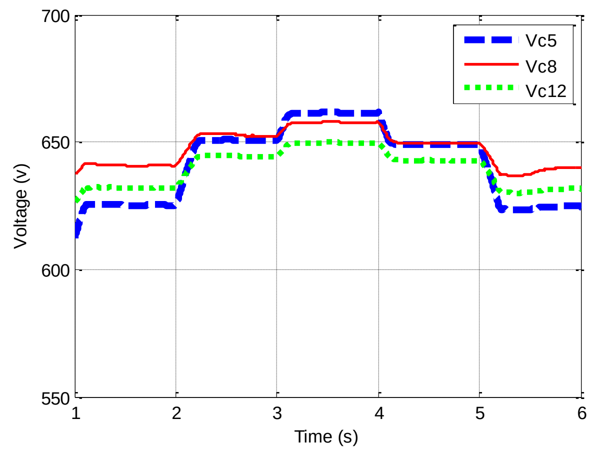

Fig. 19. Voltage variation of C_5, C_8, C_{12} by applying adaptive ST sliding mode controller

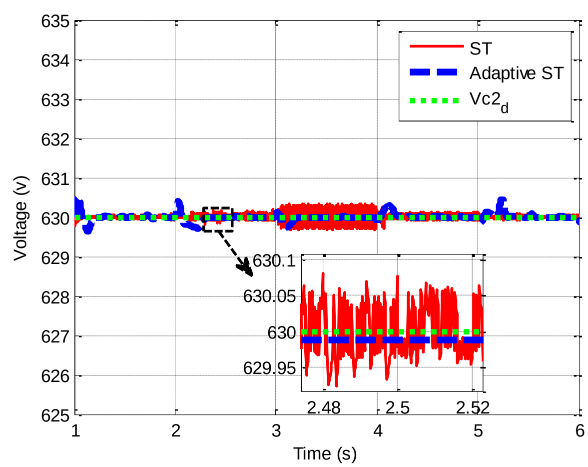

Fig. 20. Voltage variation V_{C2} and desired voltage V_{C2}* by applying adaptive ST and super twisting sliding mode controllers

Following transient events, the capacitor voltages recover more rapidly and remain tightly regulated around their reference values with minimal fluctuations. This improvement is particularly important in DC microgrid applications, where stable capacitor voltages contribute directly to enhanced power quality, reduced stress on power electronic components, and more reliable operation of interconnected loads and distributed energy resources. Overall, the results presented in Fig. 19 and 20 confirm that while both controllers achieve high tracking accuracy, the proposed AST-SMC provides superior dynamic performance by delivering smoother voltage responses, reduced oscillatory behavior, and improved robustness compared with the conventional ST controller.

As shown in **Fig. 21**, DC voltage variation is less than %5. Finally, signals inputs are shown in **Fig. 22** and proposed adaptive super twisting method has smoother control signals in comparison with ST method.

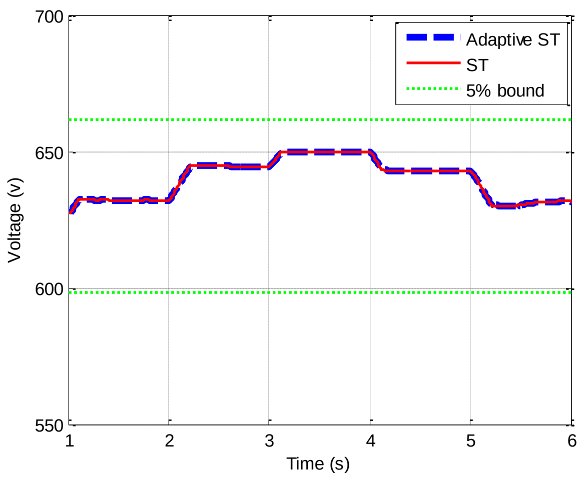

Fig. 21. Voltage variation of DC Link by applying adaptive ST and super twisting sliding mode controllers

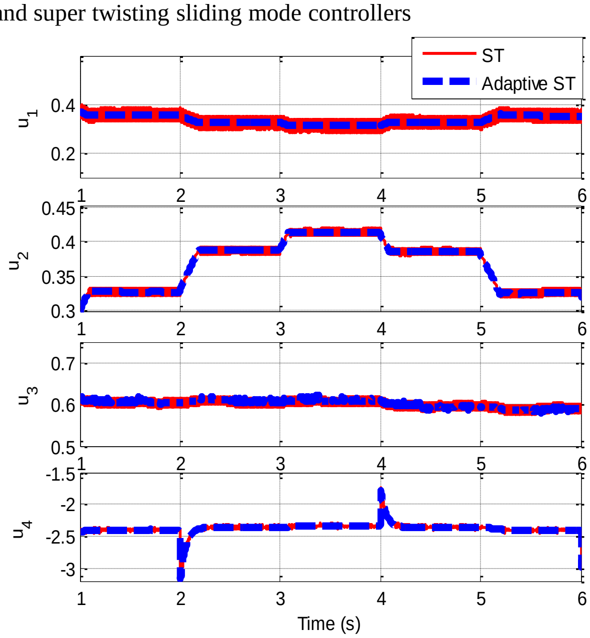

Fig. 22. Control inputs variations by applying adaptive ST and super twisting sliding mode controllers

Table 2. quantitatively compares the performance of the conventional SMC, super-twisting, and proposed adaptive super-twisting controllers. The AST controller achieves the shortest settling time and the lowest RMSE while significantly reducing chattering. The results demonstrate that online adaptation of the super-twisting gains improves tracking accuracy and disturbance rejection compared with the fixed-gain ST controller.

Table 2. comparison of the performances between SMC, ST and AST.

Method	Settling Time (s)	Overshoot (%)	RMSE (V)	Chattering Index
SMC	0.42	2.8	1.91	High
ST	0.31	1.5	1.12	Medium
AST	0.18	0.4	0.42	Low

6. Conclusions

In this article, voltage regulation in a DC micro grid was carried out by adaptive Super-Twisting sliding mode controller. Nonlinear and robust sliding mode controller was used in this paper because of nonlinearity and uncertainty in dynamic model of DC micro grid system. The utilized controller guarantees finite time stability of tracking error. Ultimately, this method was separately applied to four micro grid subsystems. Simulation results showed desirable appliance of this controller for voltage regulation in the micro grid. Also, by applying proposed method, variables and control signals had higher accuracy and smoother behavior in comparison with conventional and ST sliding mode methods. The proposed AST-SMC operates as a local controller at each DC/DC converter without requiring communication with other converters, making it inherently scalable to larger DC microgrids with multiple interconnected subsystems. In a multi-bus configuration, inter-bus coupling effects appear as additive matched disturbances and are rejected by the adaptive gain mechanism, provided the coupling magnitude remains within the disturbance bound D. Full validation of the decentralized multi-converter architecture is reserved for future work. Several extensions of the proposed framework are identified for future investigation: (i) Extension to grid-connected DC microgrids, where the control objective shifts from voltage regulation to power flow management and the bus voltage is stiffened by the utility grid. (ii) Integration with an AC frequency-regulation layer in hybrid AC/DC microgrids via interlinking converters, enabling a unified voltage and frequency control framework. (iii) Hardware-in-the-loop (HIL) validation on a real-time digital simulator (e.g., OPAL-RT or dSPACE) to confirm the real-time implementation feasibility analysis of Section 4.5. (iv) Extension of the adaptive law to handle multi-energy systems incorporating fuel cells or supercapacitors.

References

[1] Ashtari Mahini, M., Hakimi, S. M., Naghavi, S. V., & Behnamgol, V. (2025). Design of an Adaptive Super-Twisting Sliding Mode Controller to Adjust Voltage in DC Microgrids with Constant Power Load. *Iranian Journal of Science and Technology, Transactions of Electrical Engineering*, 49(1), 337-357..

[2] Thomas, T., Mishra, M. K., Kumar, C., & Liserre, M. (2024). Control of a PV-wind based DC microgrid with hybrid energy storage system using Lyapunov approach and sliding mode control. *IEEE Transactions on Industry Applications*, 60(2), 3746-3758.

[3] Saifoddin,A , Mirzaei,N , Allahrabbi Shirazi,M and Yousefi,H . (2025). Comparative Applications of Supervised and Unsupervised Machine Learning Models in Energy Systems. *Journal of Energy Management and Technology*, *9*(4), 284-290.

[4] Moaven,M , Allahrabbi Shirazi,M and Ghodusinejad,M H . (2025). Systematic Analysis of the Impact of Life Cycle Assessment of Materials on Urban Heat Island Mitigation: A Path Toward Sustainable Urban Policy Using the PRISMA Method. *Urban Development Policy Making*, *2*(1), 95-110.

[5] Allah Rabbi Shirazi, M. A. (2024). Idea generation and examination of environmental challenges of floating solar photovoltaic power plants on wetlands and its economic advantage for local communities. *Journal of sustainable Energy Systems*, *3*(1), 39-51.

[6] Mohammadali Allahrabbi Shirazi, Rahim Zahedi, Hossein Yousefi, Alireza Aslani, Environmental and damage assessment

of electric vehicles compared to internal combustion engine vehicles under various ambient temperature scenarios using the LCA approach, Energy Nexus, Volume 20, 2025, 100606, ISSN 2772-4271.

[7] Allahrabbi Shirazi,M , Yousefi,H , Fathi,A and Baneshi,M . (2027). Urban Water Sustainability through Energy-Free Fog Water Harvesting: A Review of Fog-Collecting Systems. *Urban Development Policy Making*, *3*(1), 69-94. doi: 10.22034/judpm.2025.558718.1073

[8] Seyed Mohieddin Moezzi, Mohammadali Allahrabbi Shirazi, Alireza Rajabi Zadeh Monfared, Hossein Yousefi, Comparison of classical statistical models for forecasting CO_2 emissions, GDP, and TBL cancer indicators: A comparative analysis of East and West Asia, Energy Nexus, Volume 21, 2026, 100682, ISSN 2772-4271.

[9] S. Hou, and T. Murata, "Multi-objective Demand Responding Micro Grid Dispatch Optimization based on Energy Storage Operation with Uncertain RES Power," *Lecture Notes in Engineering and Computer Science: Proceedings of The International Multi Conference of Engineers and Computer Scientists 2021*, 20-22 October, 2021, Hong Kong, pp190-195.

[10] R. Pérez-Ibacache, C. A. Silva and A. Yazdani, "Linear State-Feedback Primary Control for Enhanced Dynamic Response of AC Microgrids", *IEEE Transactions on Smart Grid*, Vol. 10, No. 3, 2019.

[11] W. Ma, S. Ouyang, "Control strategy for inverters in microgrid based on repetitive and state feedback control", *International Journal of Electrical Power & Energy Systems*, Vol. 111, 2019.

[12] H. Jafari, et al., "Improved power sharing with a back-to-back converter and state-feedback control in a utility-connected microgrid," *2018 IEEE Texas Power and Energy Conferenc*e (TPEC), College Station, 2018.

[13] M. Armin, et al., "LMI Based Robust PID Controller Design for Voltage Control of Islanded Microgrid", *Asian Journal of Control*, Vol. 20, 2018.

[14] A. B. Siddique, M. S. Munsi, S. K. Sarker, S. K. Das, M. R. Islam, "Voltage and current control augmentation of islanded microgrid using multifunction model reference modified adaptive PID controller", *International Journal of Electrical Power & Energy Systems*, Vol. 113, 2019.

[15] G. Parise, L. Martirano, M. Kermani and M. Kermani, "Designing a power control strategy in a microgrid using PID / fuzzy controller based on battery energy storage," *IEEE International Conference on Environment and Electrical Engineering and IEEE Industrial and Commercial Power Systems Europe* (EEEIC / I&CPS Europe), Milan, 2017.

[16] H. Wang, et al., "Design of a Fractional Order Frequency PID Controller for an Islanded Microgrid: A Multi-Objective Extremal Optimization Method", *Energies*, Vol. 10, 2017.

[17] M. Zolfaghari, M. Abedi and G. B. Gharehpetian, "Robust Nonlinear State Feedback Control of Bidirectional Interlink Power Converters in Grid-Connected Hybrid Microgrids," *IEEE Systems Journal*, Vol. 14, No. 1, 2020.

[18] S. Sen and V. Kumar, "Decentralized Output-Feedback-Based Robust LQR V-f Controller for PV-Battery Microgrid Including Generation Uncertainties," *IEEE Systems Journal*, doi: 10.1109/JSYST.2020.2967774, 2020.

[19] R. Heydari, et al., "Robust and Fast Voltage-Source-Converter (VSC) Control for Naval Shipboard Microgrids," *IEEE Transactions on Power Electronics*, Vol. 34, No. 9, pp. 8299-8303, 2019.

[20] T. V. Vu, D. Perkins, F. Diaz, D. Gonsoulin, C. S. Edrington, T. El-Mezyani, "Robust adaptive droop control for DC microgrids", *Electric Power Systems Research*, Vol. 146, 2017.

[21] A. Rezvani, M. Izadbakhsh, and M. Gandomkar, "Microgrid dynamic responses enhancement using artificial neural network genetic algorithm for photovoltaic system and fuzzy controller for high wind speeds", *International Journal of Numerical Modelling*, Vol. 29, 2016.

[22] K. Tan, F. Lin, C. Shih and C. Kuo, "Intelligent Control of Microgrid With Virtual Inertia Using Recurrent Probabilistic Wavelet Fuzzy Neural Network," *IEEE Transactions on Power Electronics*, Vol. 35, No. 7, 2020.

[23] S. D. Kermany, M. Joorabian, S. Deilami and M. A. S. Masoum, "Hybrid Islanding Detection in Microgrid With Multiple Connection Points to Smart Grids Using Fuzzy-Neural Network," *IEEE Transactions on Power Systems*, Vol. 32, No. 4, 2017.

[24] M. S. Mahmoud, N. M. Alyazidi, M. I. Abouheaf, "Adaptive intelligent techniques for microgrid control systems: A survey", *International Journal of Electrical Power & Energy Systems*, Vol. 90, 2017.

[25] A. Mohammadzadeh, E. Kayacan, "A novel fractional-order type-2 fuzzy control method for online frequency regulation in ac microgrid", *Engineering Applications of Artificial Intelligence*, Vol. 90, 2020.

[26] F. Perez, A. Iovine, G. Damm and P. Ribeiro, "DC microgrid voltage stability by dynamic feedback linearization," 2018 *IEEE International Conference on Industrial Technology* (ICIT), Lyon, 2018.

[27] G. Lou, W. Gu, W. Sheng, X. Song and F. Gao, "Distributed Model Predictive Secondary Voltage Control of Islanded Microgrids With Feedback Linearization," *IEEE Access*, Vol. 6, 2018.

[28] Z. Guo, S. Li, and Y. Zheng, "Feedback Linearization Based Distributed Model Predictive Control for Secondary Control of Islanded Microgrid", *Asian Journal of Control*, Vol. 22, 2020.

[29] S. Yousefizadeh, et al., "Tracking Control for a DC Microgrid Feeding Uncertain Loads in More Electric Aircraft: Adaptive Backstepping Approach," *IEEE Transactions on Industrial Electronics*, Vol. 66, No. 7, 2019.

[30] M. Cucuzzella, G. P. Incremona and A. Ferrara, "Decentralized Sliding Mode Control of Islanded AC Microgrids with Arbitrary Topology," *IEEE Transactions on Industrial Electronics*, Vol. 64, No. 8, 2017.

[31] H. R. Baghaee, M. Mirsalim, G. B. Gharehpetian and H. A. Talebi, "A Decentralized Power Management and Sliding Mode Control Strategy for Hybrid AC/DC Microgrids including Renewable Energy Resources," *IEEE Transactions on Industrial Informatics*, 2017.

[32] H. R. Baghaee, M. Mirsalim, G. B. Gharehpetian and H. A. Talebi, "Decentralized Sliding Mode Control of WG/PV/FC Microgrids Under Unbalanced and Nonlinear Load Conditions for On- and Off-Grid Modes," *IEEE Systems Journal*, Vol. 12, No. 4, 2018.

[33] T. Li, Q. Cheng, "Structure analysis and sliding mode control of new dual quasi Z source inverter in microgrid", *International Transactions on Electrical Energy Systems*", Vol. 29, 2019.

[34] T. Morstyn, A. V. Savkin, B. Hredzak and V. G. Agelidis, "Multi-Agent Sliding Mode Control for State of Charge Balancing Between Battery Energy Storage Systems Distributed in a DC Microgrid," *IEEE Transactions on Smart Grid*, Vol. 9, No. 5, 2018.

[35] P. Ge, Y. Zhu, T. Green and F. Teng, "Resilient Secondary Voltage Control of Islanded Microgrids: An ESKBF-Based Distributed Fast Terminal Sliding Mode Control Approach," *IEEE Transactions on Power Systems*, 2020.

[36] N. M. Dehkordi, N. Sadati, M. Hamzeh, "A backstepping high-order sliding mode voltage control strategy for an islanded microgrid with harmonic/interharmonic loads", *Control Engineering Practice*, Vol. 58, 2017.

[37] D. Xu, Y. Dai, C. Yang, X. Yan, "Adaptive fuzzy sliding mode

command-filtered backstepping control for islanded PV microgrid with energy storage system", *Journal of the Franklin Institute*, Vol. 356, No. 4, 2019.

[38] D. Xu, W. Zhang, B. Jiang, P. Shi and S. Wang, "Directed-Graph-Observer-Based Model-Free Cooperative Sliding Mode Control for Distributed Energy Storage Systems in DC Microgrid," *IEEE Transactions on Industrial Informatics*, Vol. 16, No. 2, 2020.

[39] H. Li, X. Wang and J. Xiao, "Adaptive Event-Triggered Load Frequency Control for Interconnected Microgrids by Observer-Based Sliding Mode Control," *IEEE Access,* Vol. 7, 2019.

[40] B. Yang, J. Wang, Y. Sang, L. Yu, H. Shu, Sh. Li, T. He, L. Yang, X. Zhang, T. Yu, "Applications of supercapacitor energy storage systems in microgrid with distributed generators via passive fractional-order sliding-mode control", *Energy*, Vol. 187, 2019.

[41] S. Chaturvedi, D. Fulwani and J. M. Guerrero, "Adaptive-Sliding-Mode-Control based Output Impedance Shaping for Ripple Management in DC Microgrids Affected by Inverter Loads," *IEEE Transactions on Sustainable Energy*, 2020.

[42] Khalil, H. K. (2002). *Nonlinear systems* (3rd ed.). Prentice Hall.

[43] Behnamgol, V., Asadi, M., Mohamed, M. A., Aphale, S. S., & Faraji Niri, M. (2024). Comprehensive review of lithium-ion battery state of charge estimation by sliding mode observers. Energies, 17(22), 5754..

[44] Behnamgol, V., Asadi, M., Aphale, S. S., & Sohani, B. (2025). Recursive PID-NT Estimation-Based Second-Order SMC Strategy for Knee Exoskeleton Robots: A Focus on Uncertainty Mitigation. *Electronics*, 14(7), 1455.

[45] V. Behnamgol, A. R. Vali, A. Mohammadi and A. Oraee, "Lyapunov-based Adaptive SmoothSecondorder Sliding Mode Guidance Law with Proving Finite Time Stability", *Journal of Space Science and Technology*, Vol. 11, No. 2, Summer 2018.

[46] Behnamgol, V., Asadi, M., & Aphale, S. S. (2025). Adaptive sliding mode control with fixed-time stability for robust glucose regulation. *International Journal of Dynamics and Control*, 13(4), 157.

[47] Kassim, S. O., Zou, J., Behnamgol, V., Vaziri, V., & Aphale, S. S. (2025). Enhancing wide-band trajectory tracking and finite-time control of Dielectric Elastomer Actuators using Nonsingular terminal sliding mode control scheme. Mechatronics, 109, 103336.

[48] F. Perez, et al., "Nonlinear Control for Isolated DC MicroGrids", *Revue Africaine de la Recherche en Informatique et Mathématiques Appliquées*, INRIA, Vol. 30, 2019.